Second-order non-linear conductance of a two-dimensional mesoscopic conductor

1998 J. Phys.: Condens. Matter 10 5335

(http://iopscience.iop.org/0953-8984/10/24/011)

J. Phys.: Condens. Matter **10** (1998) 5335–5350. Printed in the UK PII: S0953-8984(98)91953-1

Second-order non-linear conductance of a two-dimensional mesoscopic conductor

Wei-Dong Sheng†§, Jian Wang† and Hong Guo‡

† Department of Physics, The University of Hong Kong, Pokfulam Road, Hong Kong
‡ Centre for the Physics of Materials, Department of Physics, McGill University, Montreal, Quebec, Canada H3A 2T8

Received 28 February 1998

Abstract. We have investigated the weakly non-linear quantum transport properties of a two-dimensional quantum conductor. We have developed a numerical scheme which is very general for this purpose. The second-order non-linear conductance is computed for the first time for a truly two-dimensional structure by explicitly evaluating the various partial densities of states, the sensitivity and the characteristic potential. Interesting spatial structures of these quantities are revealed. We present detailed results concerning the crossover behaviour of the second-order non-linear conductance, occurring when the conductor changes from geometrically symmetrical to asymmetrical. Other issues of interest such as the gauge invariance are also discussed.

1. Introduction

Non-linear phenomena in electric conduction play the most important role in many electronic device applications, the devices ranging from single units such as a diode or a transistor to entire circuits. For extremely small systems with mesoscopic or atomic length scales, such as those which can now be routinely fabricated using nanotechnology, quantum transport dominates the conduction. While we now have a very good understanding of linear quantum transport phenomena in nanosystems where quantum coherence plays a vital role, the non-linear quantum transport properties of mesoscopic conductors have received less attention. However, several important research results have been reported in recent years [1–5]. On the experimental side, Taboryski *et al* [5] have reported observations of non-linear and asymmetric conductance oscillations in quantum point contacts at small bias voltages. They found that the non-Ohmic and asymmetric behaviour causes a rectified DC signal as the response to an applied AC current. On the theoretical side, several directions have been explored. Wingreen *et al* [3] have presented a general formulation for dealing with the situation of a non-linear and time-dependent current going through a small interacting region where electron energies can be changed by time-dependent voltages. de Vegvar [4] has studied the low-frequency second-harmonic transport response of multiprobe mesoscopic conductors using perturbation theory in the framework of the Kubo formula and found that the low-frequency second-harmonic current is a non-Fermi-surface quantity. At the same time, Büttiker and co-workers [6, 1, 7] have advanced a current-conserving theory for the frequency-dependent transport. This theory can be applied in discussing the non-linear behaviour of mesoscopic samples. It has been recognized [8] that in non-linear coherent

§ Present address: Department of Solid State Physics, University of Lund, Box 118, S-22100 Lund, Sweden.

0953-8984/98/245335+16$19.50

quantum transport, it is essential to consider the internal self-consistent potential in order to have the theory satisfy the gauge-invariant condition. This is a fundamental condition, which requires that none of the physical properties predicted by a theory can change if there is a global voltage shift. Recently, Christen and Büttiker [8] have investigated the rectification coefficient of a quantum point contact and the non-linear current–voltage characteristic of a resonant level in a double-barrier structure by assuming the scattering matrix to be of Breit–Wigner form.

Clearly it is important and useful to investigate non-linear quantum transport phenomena in coherent quantum conductors further and numerically implement the existing theory of non-linear conductance. In particular, detailed predictions of non-linear conductance of two-dimensional (2D) systems warrant making because such systems can now be fabricated in many laboratories. Unfortunately, due to various technical difficulties, especially the difficulty of evaluating a quantity called the *sensitivity* (see below), so far the application of Büttiker's non-linear theory [8] has largely been limited to quasi-1D systems. The non-linear conductance for a 2D conductor, on the other hand, has been investigated for a very special and exactly solvable model, namely that of a quasi-1D ballistic wire with a δ-function impurity confined inside [9]. Since it is exactly solvable, the sensitivity can be computed in a closed form, thereby overcoming the technical difficulties associated with the theoretical formalism. To the best of our knowledge, this is the only explicit computation of the weakly non-linear conductance from the gauge-invariant AC transport theory that has been carried out for a 2D system, where mode mixing is the most important characteristic. However, we note that in order to apply the theoretical formalism to a wide range of 2D mesoscopic conductors, a more general numerical method must be developed and various physical issues clarified. The purpose of this article is to report our development of such a numerical method, and to investigate the weakly non-linear transport properties of a truly 2D system with mode-mixing characteristics.

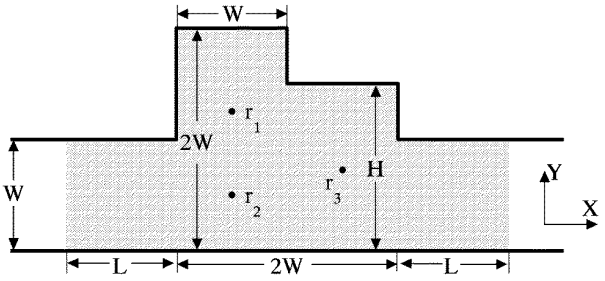

Figure 1. A schematic view of an asymmetric cavity (the shaded area) embedded in a quantum wire.

As we have noted from the previous investigation of the exactly solvable model [9], for a geometrically symmetric system the second-order non-linear conductance G_{111} must be zero from a general symmetry argument. Hence the non-linear effect, i.e. a non-zero $G_{\alpha\beta\gamma}$, obtained in reference [9] is a delicate effect of the asymmetric scattering boundary [10]. Such an asymmetry is brought about when the δ-function scatterer is not located at the centre of the scattering volume [9]. Very interesting and physically revealing behaviour of the local current response (the sensitivity) has already been found. In this work, on the other hand, we shall focus on a much more general situation, by investigating the 2D conductor depicted in figure 1 which is a quasi-1D quantum wire with a side stub.

An important system parameter to be specified for non-linear analysis is the scattering

volume; for the conductor of figure 1 it is defined by the shaded area. By 'scattering volume' we specifically mean the space in which electron–electron (ee) interactions will be considered, i.e. the self-consistent internal potential response will be calculated for this volume. In principle, one needs to consider the limit $L \to \infty$ (see figure 1); however, in numerical analysis that limit is achieved when L is sufficiently large that the scattering volume boundary is far away from the side-stub region (see below and the discussion in section 4). The two leads, of width W, are assumed to extend far away from the scattering volume. The shape of the side stub is controlled by the parameter H as shown in figure 1, and hence various different 2D systems can be generated by varying H. When $H = 2W$, the scattering volume is geometrically symmetric, and hence the non-linear conductance $G_{\alpha\beta\gamma}$ must be zero. Similarly, when $H = W$ and $L \to \infty$, the system is symmetric, and thus $G_{\alpha\beta\gamma}$ vanishes. For other values of H between W and $2W$, the scattering volume is intrinsically asymmetric where a finite $G_{\alpha\beta\gamma}$ is expected. By varying H, we shall study the crossover behaviour of G_{111} between the symmetric and asymmetric situations. Finally, a point of academic interest arises for $H = W$ but with a finite L: in this case the scattering volume is geometrically asymmetric (see figure 1) but this asymmetry is only due to the *asymmetric* location of the scattering volume boundary, which is artificially chosen. Nevertheless, a small but finite G_{111} is expected with a behaviour similar to that discussed in reference [9].

Our results show that the external (the internal) response of the second-order non-linear conductance changes sign from negative (positive) to positive (negative) near a quantum resonant point. The cancellation of the external and internal responses results in a much smaller second-order non-linear conductance G_{111}, i.e., G_{111} is one order of magnitude smaller than the external or internal response. This is an important result and it indicates that theories in which the internal response is not taken into consideration self-consistently will not only violate gauge invariance, but also give incorrect numerical results. The behaviour of G_{111} is non-monotonic when the parameter H is varied in the range $W \leqslant H \leqslant 2W$: this is because G_{111} is very small at $H = W$ as it is solely due to the asymmetric scattering boundary, it increases as H is increased, and it is zero at $H = 2W$. Another result of our analysis concerns the gauge invariant condition $\sum_\gamma G_{\alpha\beta\gamma} = 0$. It turns out that for systems with a finite scattering volume such as those in any numerical calculations, if the global partial density of states (GPDOS) is computed from the *energy* derivatives of the scattering matrix, then it is the case [9] that a correction term must be added to satisfy the gauge-invariant condition. For the exactly solvable model studied in our previous work [9], this correction term has been derived analytically. We shall examine this effect for the conductor studied here.

The paper is organized as follows. In the next section we shall briefly review the gauge-invariant theory for non-linear transport developed by Büttiker [1]. The method of calculating various quantities needed for studying non-linear conductance and our results are presented in sections 3 and 4. The last section serves as a brief summary.

2. The formalism

The gauge-invariant formalism of non-linear transport has been developed and clearly discussed in reference [8] and we refer the interested reader to the original work. In this section, we shall outline the main steps of the application of this formalism for our calculation. In the weakly non-linear regime, the current of a two-probe conductor is given by

$$I_1 = G_{11}(V_1 - V_2) + G_{111}(V_1 - V_2)^2 \tag{1}$$

where G_{11} is the usual linear conductance and G_{111} is the second-order non-linear conductance. As shown in reference [8], $G_{\alpha\beta\gamma}$ consists of two terms:

$$G_{\alpha\beta\gamma} = G^e_{\alpha\beta\gamma} + G^i_{\alpha\beta\gamma} \tag{2}$$

where the external contribution can be obtained using the free-electron scattering theory by evaluating the energy derivatives of the scattering matrix:

$$G^e_{\alpha\beta\gamma} = \frac{e^2}{h}\int \mathrm{d}E\ (-\partial_E f) e\,\partial_E A_{\alpha\beta}\,\delta_{\beta\gamma} \tag{3}$$

where

$$A_{\alpha\beta}(E,\{V_\gamma\}) = \mathrm{Tr}[\mathbf{1}_\alpha\delta_{\alpha\beta} - \mathbf{s}^\dagger_{\alpha\beta}(E,\{V_\gamma\})\mathbf{s}_{\alpha\beta}(E,\{V_\gamma\})] \tag{4}$$

are the screened (negative) transmission functions which are expressed in terms of the scattering matrix $\mathbf{s}_{\alpha\beta}$. The internal contribution, on the other hand, is much more difficult to obtain because it depends on the potential derivatives of the scattering matrix:

$$G^i_{\alpha\beta\gamma} = \frac{e^2}{h}\int \mathrm{d}E\ (-\partial_E f)(\partial_{V_\gamma} A_{\alpha\beta} + \partial_{V_\beta} A_{\alpha\gamma}). \tag{5}$$

This is difficult to evaluate because when the voltage of a probe V_γ changes, the entire potential landscape of the scattering volume will change accordingly through the electron–electron interactions. Hence the internal contribution to the non-linear conductance can be obtained only after an interacting electron problem has been solved [8]. This is a very difficult task and so far has not been successfully implemented in a numerical scheme. However, if we can use the Thomas–Fermi linear screening model, which is more appropriate for metallic conductors, the internal contribution can be computed through the evaluation of quantities called the sensitivity and the characteristic potential [8]. It can be shown [8] that the potential derivative of the transmission function is given as

$$\partial_{V_\gamma} A_{\alpha\beta} = 4\pi\int \mathrm{d}^3\boldsymbol{r}\ \eta_{\alpha\beta}(\boldsymbol{r})u_\gamma(\boldsymbol{r}) \tag{6}$$

where

$$\eta_{\alpha\beta}(\boldsymbol{r}) = \frac{1}{4\pi}\frac{\delta A_{\alpha\beta}}{\delta U(\boldsymbol{r})} = -\frac{1}{4\pi}\,\mathrm{Tr}\left(\mathbf{s}^\dagger_{\alpha\beta}\frac{\delta \mathbf{s}_{\alpha\beta}}{\delta U(\boldsymbol{r})} + \mathbf{s}_{\alpha\beta}\frac{\delta \mathbf{s}^\dagger_{\alpha\beta}}{\delta U(\boldsymbol{r})}\right) \tag{7}$$

is called the *sensitivity* [12], which measures the local electric current response to an external perturbation. $u_\gamma(\boldsymbol{r})$ is the characteristic potential, which measures the variation of the potential landscape of the scattering volume due to the perturbation [1]. Within the Thomas–Fermi screening model, it is given by [7, 11]

$$u_\gamma(\boldsymbol{r}) = \frac{\mathrm{d}n(\boldsymbol{r},\gamma)}{\mathrm{d}E}\Big/\frac{\mathrm{d}n(\boldsymbol{r})}{\mathrm{d}E}.$$

Here $\mathrm{d}n(\boldsymbol{r},\gamma)/\mathrm{d}E$ and $\mathrm{d}n(\boldsymbol{r})/\mathrm{d}E$ are local partial densities of states which will be discussed in the next section.

On the basis of the weakly non-linear conductance formalism summarized above, several observations are in order. First, if one is applying this formalism, a crucial step is the evaluation of the sensitivity $\eta_{\alpha\beta}$, which depends on the functional derivative of the scattering matrix with respect to the local potential variation. The latter is caused by the external perturbation, i.e. the change of the electrochemical potential at a lead. We are aware of two ways of calculating the sensitivity [12]. The first is to evaluate $\delta\mathbf{s}_{\alpha\beta}/\delta U$ directly by introducing a δ-function of infinitesimal strength δU inside the scattering region. Alternatively, one can calculate it using the retarded Green's function. For a 2D system,

in general the Green's function cannot be obtained explicitly except in very special cases; hence we shall use the first method and directly compute the sensitivity. As a second observation which is physically important [10], we can discuss the general behaviour of the non-linear conductance G_{111}. From equation (1), for a symmetric scattering volume with scattering potential $U(x, y) = U(-x, y)$ where x is the propagation direction, we must obtain $-I_1$ if V_1 and V_2 are interchanged. Hence we conclude that for a symmetric scattering volume there are no quadratic terms, i.e., $G_{111} = 0$. On the other hand, in general $G_{111} \neq 0$ for geometrically asymmetrical systems. Finally, due to the current conservation and the gauge-invariant condition—namely that the entire physics is as a whole unaffected by a global voltage shift—it is not difficult to prove [1, 8, 13] that

$$\sum_{\alpha} G_{\alpha\beta\gamma} = \sum_{\beta} G_{\alpha\beta\gamma} = \sum_{\gamma} G_{\alpha\beta\gamma} = 0. \tag{8}$$

Our results will allow a direct confirmation of this equation.

3. The numerical method

There are several ways to solve the scattering matrix of 2D ballistic conductors, such as the mode-matching method [14], the recursive Green's function method [15–18] and the finite-element method [18, 19]. However, we found that none of these methods is very easy to apply here, because we need not only the scattering matrix, but also the sensitivity $\eta_{\alpha\beta}$. In view of this, we shall discuss in this section our numerical procedure for finding $\eta_{\alpha\beta}$ using the scattering matrix method.

In particular, we construct a global scattering matrix using the mode-matching method of reference [20]. If a scattering volume is not uniform along its longitudinal direction, we divide it into a number of uniform sections; e.g., the asymmetric cavity shown in figure 1 can be divided into four uniform sections. The scattering matrix associated with the nth section $\mathbf{S}_n$ is the composition of two individual scattering matrices $\mathbf{S}_n^f$ and $\mathbf{S}_n^i$, i.e., $\mathbf{S}_n = \mathbf{S}_n^f \otimes \mathbf{S}_n^i$ where $\otimes$ is the operator which denotes the composition of two scattering matrices [21]. Here $\mathbf{S}_n^f$ describes the free propagation from the left-hand end of the nth section to its right-hand end. The scattering process at the interface between two adjacent sections (the nth and $(n+1)$th sections) is described by $\mathbf{S}_n^i$. Care must be taken when matching the wavefunctions of two sections with different widths at the section boundary [20]. If the width of the nth section W_n is not greater than W_{n+1}, we have

$$\mathbf{S}_n^i = \begin{bmatrix} -\mathbf{C}^{\mathrm{T}} & \mathbf{I} \\ \mathbf{K}_n & \mathbf{C}\mathbf{K}_{n+1} \end{bmatrix}^{-1} \begin{bmatrix} \mathbf{C}^{\mathrm{T}} & -\mathbf{I} \\ \mathbf{K}_n & \mathbf{C}\mathbf{K}_{n+1} \end{bmatrix} \tag{9}$$

where $\mathbf{K}_n$ is a diagonal matrix with diagonal elements k_n^m, where k_n^m is the longitudinal wavenumber for the mth mode, and $\mathbf{I}$ is a unit matrix. $\mathbf{C}$ is a matrix which denotes the coupling between the transverse modes in the two sections and its elements are given by $C_{ij} = \langle \phi_n^i | \phi_{n+1}^j \rangle$ where ϕ_n^i is the ith transverse mode in the nth section. $\mathbf{C}^{\mathrm{T}}$ is the transpose of the matrix $\mathbf{C}$. On the other hand, if $W_n > W_{n+1}$, we have

$$\mathbf{S}_n^i = \begin{bmatrix} -\mathbf{I} & \mathbf{C} \\ \mathbf{C}^{\mathrm{T}}\mathbf{K}_n & \mathbf{K}_{n+1} \end{bmatrix}^{-1} \begin{bmatrix} \mathbf{I} & -\mathbf{C} \\ \mathbf{C}^{\mathrm{T}}\mathbf{K}_n & \mathbf{K}_{n+1} \end{bmatrix}. \tag{10}$$

Once the scattering matrices for each of the sections are is known, the global scattering matrix can be easily constructed by the composition of all of the individual scattering matrices:

$$\mathbf{S} = \mathbf{S}_1 \otimes \mathbf{S}_2 \otimes \ldots \otimes \mathbf{S}_{M-1} \tag{11}$$

where M is the total number of sections.

The above procedures can easily be modified to compute the sensitivity $\eta_{\alpha\beta}(\boldsymbol{r})$. For this purpose, we shall make use of a δ-function impurity to calculate the functional derivatives of the scattering matrices $\delta\mathbf{s}_{\alpha\beta}/\delta U(\boldsymbol{r})$. This is achieved as follows. We put a δ-function impurity with infinitesimal strength γ, $V(\boldsymbol{r}) = \gamma\delta(\boldsymbol{r} - \boldsymbol{r}_0)$, at arbitrary positions $\boldsymbol{r} = \boldsymbol{r}_0$ in the scattering volume. We then calculate the scattering matrix $\mathbf{s}_{\alpha\beta}$ as a function of γ. Finally we use a five-point numerical derivative to evaluate $\delta\mathbf{s}_{\alpha\beta}/\delta U(\boldsymbol{r}) \equiv \partial\mathbf{s}_{\alpha\beta}/\partial\gamma|_{\gamma=0}$. With this result we can obtain the sensitivity from equation (7).

The scattering matrix can still be obtained using the approach discussed above even including the δ-function impurity [21, 22]. Suppose the δ-function impurity is located in the nth section at position $\boldsymbol{r}_0 = (x_0, y_0)$, where x_0 and y_0 are the distances from the left-hand and bottom boundaries of the section, respectively. The scattering matrix associated with this section is then given by

$$\mathbf{S}_n = \mathbf{S}_n^f(x_0) \otimes \mathbf{S}_n^\delta \otimes \mathbf{S}_n^f(L_n - x_0) \otimes \mathbf{S}_n^i \tag{12}$$

where $\mathbf{S}_n^\delta$ describes the scattering process associated with the δ-function impurity and is given by [22]

$$\mathbf{S}_n^\delta = \begin{bmatrix} -\mathbf{I} & \mathbf{I} \\ \mathrm{i}\mathbf{K}_n - \boldsymbol{\Gamma} & \mathrm{i}\mathbf{K}_n \end{bmatrix}^{-1} \begin{bmatrix} \mathbf{I} & -\mathbf{I} \\ \mathrm{i}\mathbf{K}_n + \boldsymbol{\Gamma} & \mathrm{i}\mathbf{K}_n \end{bmatrix} \tag{13}$$

where the matrix $\boldsymbol{\Gamma}$ describes the mode-mixing effect due to the δ-function impurity and its matrix elements are given by $\Gamma_{pq} = 2\gamma \sin(p\pi y_0/W_n)\sin(q\pi y_0/W_n)/W_n$ with W_n being the width of the section. With the δ-function included this way, we can again apply equation (11) to compute the scattering matrix $\mathbf{s} = \mathbf{s}(\gamma)$ and complete the numerical derivatives discussed in the last paragraph.

To end this section, we briefly mention two other points. First, the characteristic potential is evaluated using the scattering wavefunction which can be calculated in two ways, directly or indirectly. One can directly compute the wavefunction using the mode-matching method [14] or the finite-element method [18, 19]. Or one can compute the wavefunction ($|\Psi|^2$) indirectly by computing the local partial DOS, called the emissivity, defined as [13]

$$\frac{\mathrm{d}n(\alpha, \boldsymbol{r})}{\mathrm{d}E} = -\frac{1}{4\pi\,\mathrm{i}} \sum_\beta \mathrm{Tr}\left(\mathbf{s}_{\alpha\beta}^\dagger \frac{\delta\mathbf{s}_{\alpha\beta}}{\delta e U(\boldsymbol{r})} - \mathbf{s}_{\alpha\beta} \frac{\delta\mathbf{s}_{\alpha\beta}^\dagger}{\delta e U(\boldsymbol{r})} \right). \tag{14}$$

In the absence of a magnetic field, the micro-reversibility of the scattering matrix implies that

$$\frac{\mathrm{d}n(\alpha, \boldsymbol{r})}{\mathrm{d}E} = \frac{\mathrm{d}n(\boldsymbol{r}, \alpha)}{\mathrm{d}E} \tag{15}$$

where $\mathrm{d}n(\boldsymbol{r}, \gamma)/\mathrm{d}E$ is the injectivity and is given by [13] the scattering wavefunctions:

$$\frac{\mathrm{d}n(\boldsymbol{r}, \gamma)}{\mathrm{d}E} = \sum_n \frac{|\Psi_{\gamma n}(\boldsymbol{r})|^2}{h v_{\gamma n}} \tag{16}$$

where $v_{\gamma n}$ is the electron velocity for the propagating channel labelled n. We will use equations (16), (14) and (15) to compute the wavefunction $|\Psi|^2$, since we have to compute the scattering matrix or $\delta\mathbf{s}/\delta U(\boldsymbol{r})$ anyway for the sensitivity. Second, the energy derivatives of the transmission function, which determines the external response contribution to the second-order non-linear conductance, are evaluated using a five-point numerical difference method.

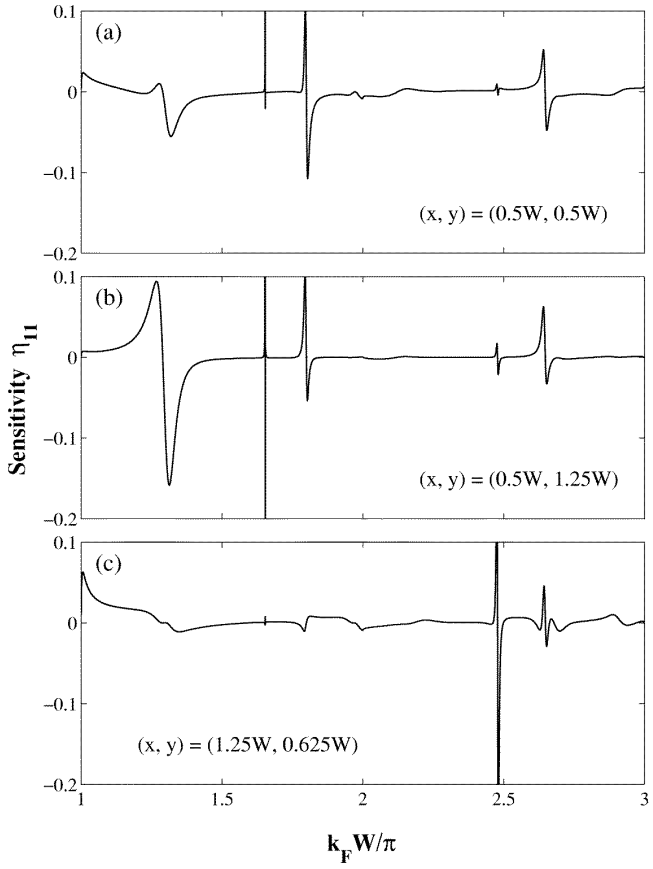

Figure 2. The sensitivity η_{11} at three different positions, $(x, y) = \{(0.5W, 0.5W), (0.5W, 1.25W), (1.25, 0.625W)\}$, as a function of the normalized electron momentum $k_F W/\pi$ for $H = 1.25W$ and $L = W$. For each curve the energy scan contains 4000 points; this large number of points was used in order to reveal the fine resonance pattern.

4. Results

As a first result, we plot in figure 2 the sensitivity $\eta_{11}(\boldsymbol{r})$ at three different positions inside the scattering volume, $\boldsymbol{r}_1 = (0.5W, 0.5W)$, $\boldsymbol{r}_2 = (0.5W, 1.25W)$ and $\boldsymbol{r}_3 = (1.25W, 0.625W)$, as a function of the normalized electron momentum $k_F W/\pi$ where k_F is the electron Fermi wavenumber. These results are for an asymmetric system (see figure 1) with the parameter $H = 1.25W$. As discussed in section 2, $\eta_{\alpha\beta}$ appears naturally in the theoretical formalism, and it essentially describes the local (internal) electric current response of the scattering problem when there is a small local potential change. It is related to the real part of the diagonal elements of the scattering Green's function [12]. From figure 2, we see that different positions inside the scattering volume have quite different internal responses in terms of the peak heights of the apparent resonance behaviour. On the other hand, the peak positions occur at the same electron energies, given by $k_F W/\pi$, for η_{11} at all three positions. We have checked (see below and figure 5(b), later) that the peak positions also coincide with those of the conductance. Hence we may conclude that the local current response can exhibit sharp changes, from positive values to negative values, across the energy of

a resonance which also mediates a resonance transmission. For the two positions $\boldsymbol{r}_1$ and $\boldsymbol{r}_2$ which are located in the left-hand part of the cavity, the shapes of the sensitivities are more similar to each other. This is to be compared with the shape of the sensitivity of the position $\boldsymbol{r}_3$ which is located in the right-hand part of the cavity. The differences are evident from the three curves of figure 2.

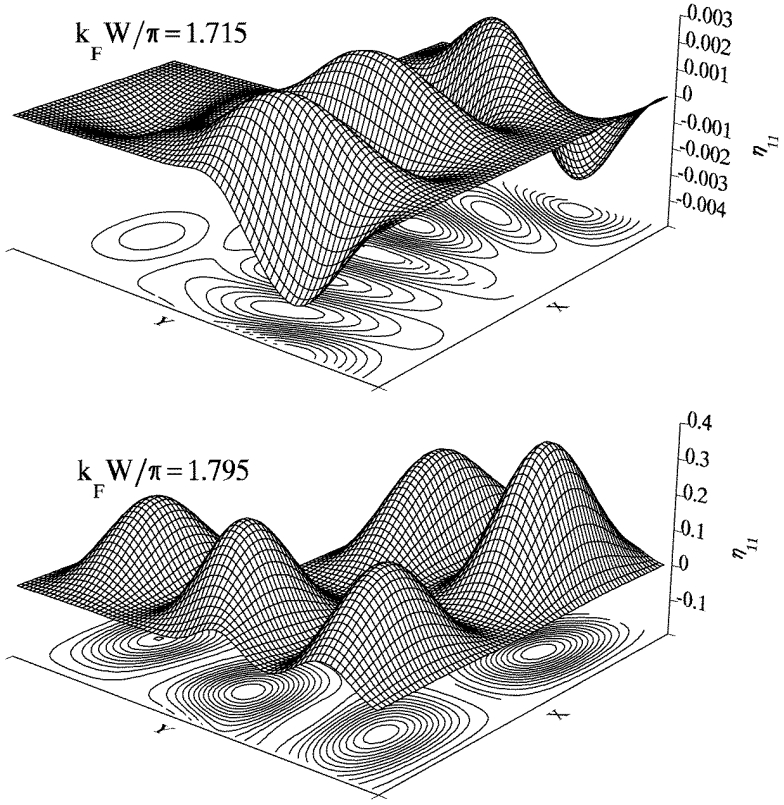

Figure 3. Three-dimensional views of the sensitivity η_{11} for $H = 1.25W$ and $L = W$ at two different values of the electron momentum, $k_F W/\pi = 1.715$ and $k_F W/\pi = 1.795$.

To get a more intuitive picture of the spatial dependence of the sensitivity, in figure 3 we plot $\eta_{11}(\boldsymbol{r})$ for the entire scattering volume for two different values of the electron momentum ($H = 1.25W$). The first case is for $k_F W/\pi = 1.715$, which is off resonance, while the second is for $k_F W/\pi = 1.795$, which is on resonance. From the lower panel of figure 3 which corresponds to the resonant energy, the behaviour of η_{11} is seen to be reminiscent of a standing wave, which is in accordance with our usual picture of a quantum resonance. The positions $\boldsymbol{r}_1$ and $\boldsymbol{r}_2$ of figure 2 are located at peaks of the sensitivity profile while $\boldsymbol{r}_3$ is in a valley. This explains why in figure 2 we observe the large resonant peaks at $\boldsymbol{r}_1$ and $\boldsymbol{r}_2$ but not at $\boldsymbol{r}_3$. For the off-resonance case, the upper panel of figure 3 shows less regular patterns for η_{11}. Hence the local current response can behave regularly or less regularly according to whether the electron Fermi energy is on or off quantum resonance for the scattering cavity. In comparison, for both 1D and 2D scattering problems involving a δ-potential barrier, the sensitivity has been derived analytically in references [12] and [9]. There, η_{11} shows strong regular spatial oscillations.

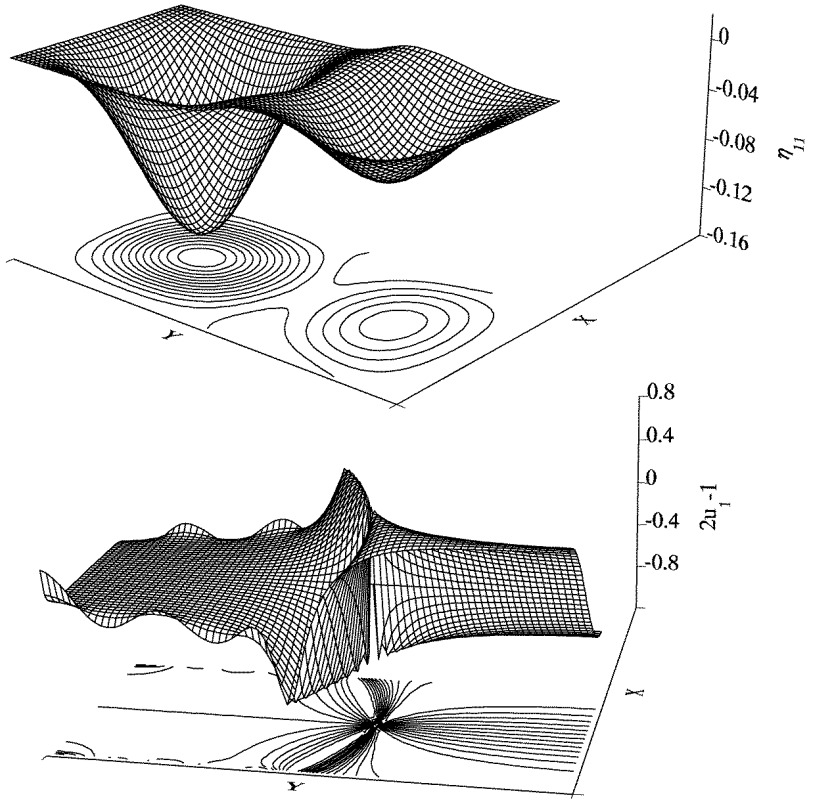

Figure 4. Three-dimensional views of the sensitivity η_{11} and the characteristic potential $2u_1 - 1$ for a symmetric T-shaped cavity at $k_F W/\pi = 1.325$, for $H = W$ and $L = W$.

When the geometry parameter $H = W$, the conductor becomes a T-shaped junction. The upper panel of figure 4 shows η_{11} for this situation at $k_F W/\pi = 1.325$. The lower panel of figure 4 plots the characteristic potential $2u_1(\boldsymbol{r}) - 1$ for this case. The quantity $2u_1(\boldsymbol{r}) - 1$ is interesting because it can easily be shown [8], using equations (2), (3), (5) and applying the gauge-invariant condition (8), that the non-linear conductance can be rewritten as

$$G_{\alpha\beta\gamma} = 4\pi \frac{e}{h} \int \mathrm{d}E \; (-\partial_E f) \int \mathrm{d}^3\boldsymbol{r} \; (\eta_{\alpha\beta} u_\gamma(\boldsymbol{r}) + \eta_{\alpha\gamma} u_\beta(\boldsymbol{r}) - \eta_{\alpha\beta}\delta_{\gamma\beta}). \tag{17}$$

Hence the quantity $2u_1(\boldsymbol{r}) - 1$ appears naturally in this form of G_{111}. From figure 4 it is clear that η_{11} is symmetric and $2u_1 - 1$ is anti-symmetric along the x-axis. As a result, G_{111} will be zero for this T-shaped junction if the scattering volume is symmetric, due to the spatial integration of equation (17). To systematically investigate the behaviour of G_{111} as the conductor shape changes from symmetric to asymmetric, we have calculated this quantity for several values of the geometric parameter H at zero temperature: $H = W$, $1.25W$, $1.5W$ and $1.75W$ (see figure 1). In figures 5(a)–5(d) we have plotted the DC conductance G_{11}, the external and internal responses of the second-order non-linear conductance, G^e_{111} [23], G^i_{111}, and G_{111} as a function of the normalized electron momentum $k_F W/\pi$ for these configurations. Since the sensitivity exhibits strong position dependence, we have used the Gaussian quadrature method in the integration of equation (17) and a careful convergence

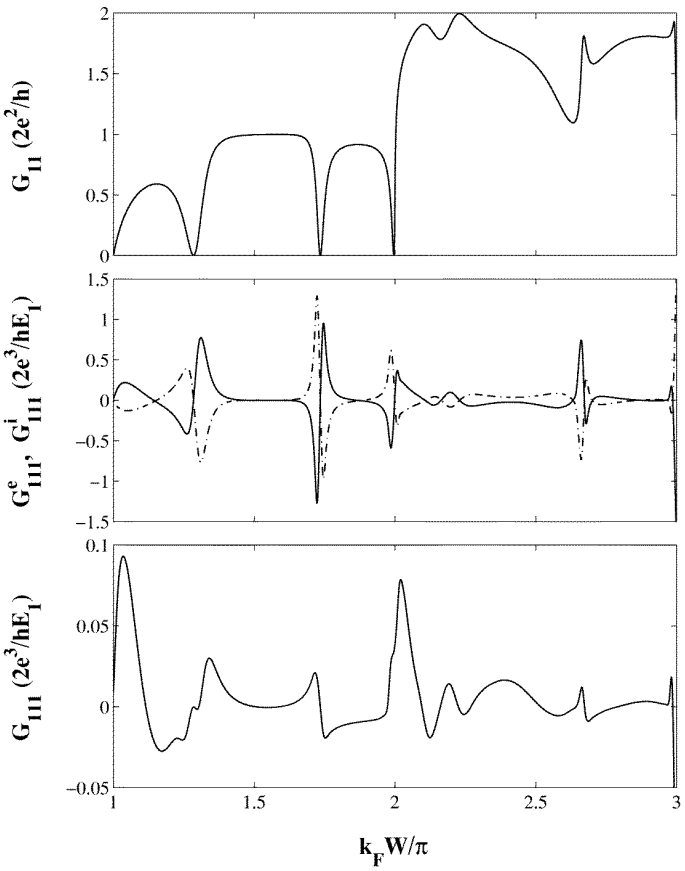

Figure 5. The DC conductances G_{11} and the leading-order non-linear terms G_{111} as a function of the normalized electron momentum $k_F W/\pi$; solid lines are for G^e_{111} and dotted lines are for G^i_{111}. (a) $H = W$, (b) $H = 1.25W$, (c) $H = 1.5W$, (d) $H = 1.75W$. Here E_1 is the threshold of the first subband, defined as $E_1 = \hbar^2\pi^2/(2mW^2)$, and $L = W$.

check has been made to achieve sufficient accuracy. Several interesting features have been observed. First of all, the external (the internal) response of the second-order non-linear conductance changes sign from negative (positive) to positive (negative) near the resonant point. This behaviour is similar to that of one-dimensional asymmetric double-barrier resonant tunnelling [8]. In that case, $G_{111} = (e^3/h)(\mathrm{d}T/\mathrm{d}E)(\Gamma_2 - \Gamma_1)/\Gamma$, where T is the transmission coefficient, Γ_i is the decay width of each barrier and $\Gamma = \Gamma_1 + \Gamma_2$. Because of the presence of the term $\mathrm{d}T/\mathrm{d}E$, G_{111} changes sign across the resonant point and hence can be negative. The cancellation of the external and internal responses results in a much smaller G_{111}: one order of magnitude smaller than the internal or external contribution alone. Secondly, for $H = W$ the asymmetry of the scattering volume only arises from the location of the scattering volume boundary, which we are free to select, and G_{111} has the smallest values for all $H < 2W$ studied. For $W < H < 2W$, the conductor is intrinsically asymmetric and the G_{111} are larger. Also, the resonance behaviour of G_{111} becomes substantially sharper as H is increased. While G_{111} increases as H increases from $H = W$, it eventually starts to decrease after $H > 1.5W$. This is clearly seen from

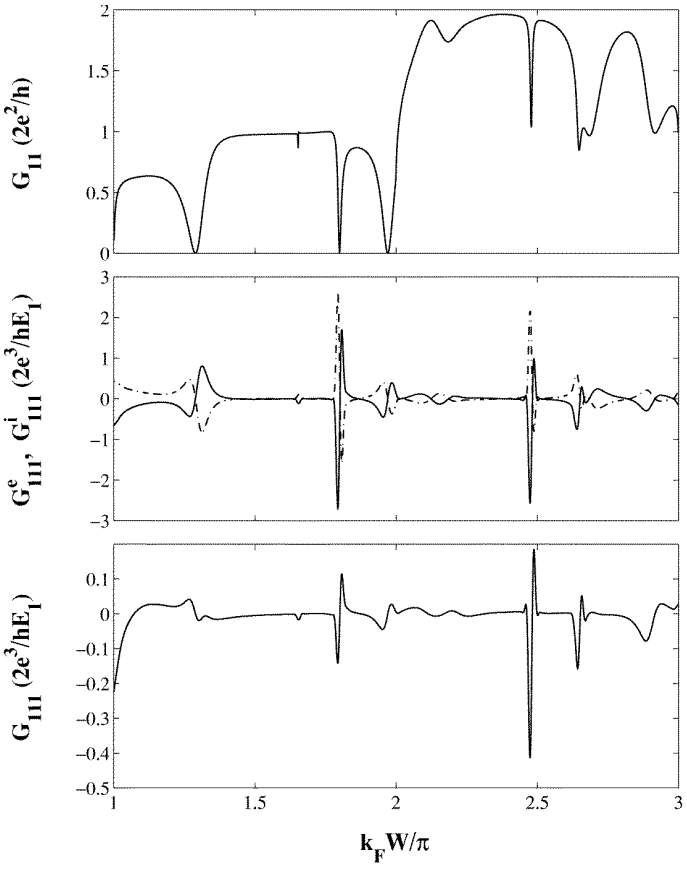

(b)

Figure 5. (Continued)

figure 5(d) for which $H = 1.75W$. This is because for larger H the system approaches being a symmetric conductor at $H = 2W$, for which $G_{111} = 0$ as discussed above.

So far, as noted in reference [23], we have computed the external contribution G^e_{111} of equation (3) using a procedure which employs the gauge-invariant condition. However, if we directly use the right-hand side of equation (3) to compute G^e_{111}, the result will not be accurate because the scattering volume is finite. In particular, as found from a previous study [9] for a symmetric system, G_{111} will be non-zero if calculated using the right-hand side of equation (3). In terms of the gauge-invariant condition, this will lead to a violation, i.e. $G_{111} + G_{112} \neq 0$. While such an error is not relevant if the scattering volume is very large, for our numerical calculations it will lead to incorrect conclusions since the scattering volume is always finite. Hence, in order to use the right-hand side of equation (3) to compute G^e_{111}, a correction term is needed to preserve the gauge invariance.

For a quasi-1D wire with a δ-function impurity, this correction term has been derived [9] analytically. For that situation, the correction, C, consists of two terms [9]:

$$C = \frac{|s_{12}|^2}{k_1^2}\,\mathrm{Re}(s_{11}) + \mathrm{Re}\left(\sum_{n=2}\frac{b_1|b_n|^2}{k_1 k_n}\mathrm{e}^{\mathrm{i}k_n(x_2-x_1)}\right) \tag{18}$$

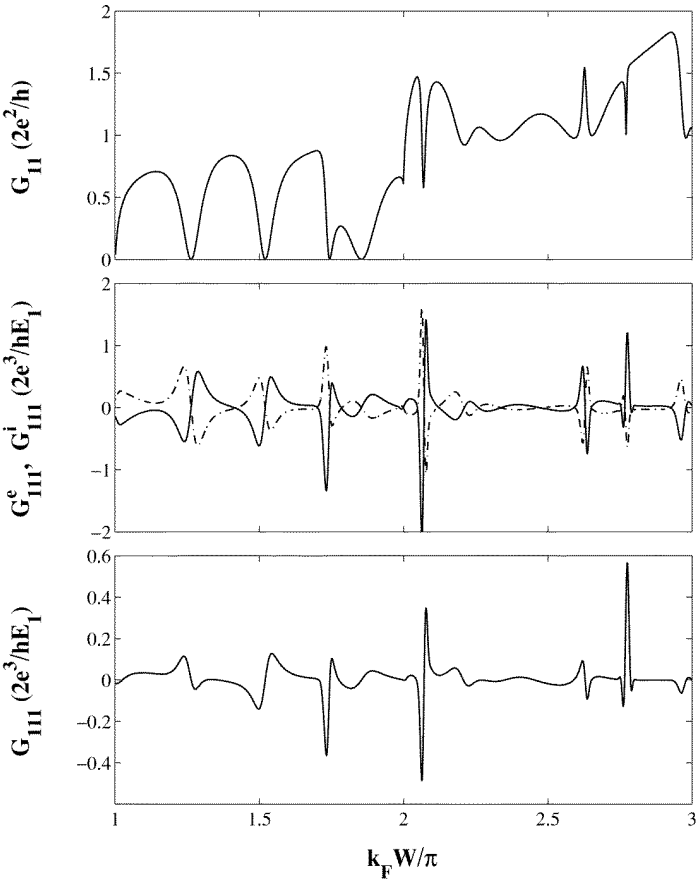

(c)

Figure 5. (Continued)

where k_n is the longitudinal momentum for the nth mode with $k_n^2 = k_F^2 - (n\pi/W)^2$ and $E = \hbar^2 k_F^2/2m$, x_1 and x_2 are the coordinates for the scattering boundaries, and b_n is the reflection scattering amplitude. Clearly, the first term is oscillating as the linear size of the scattering volume increases (due to s_{11}) and it is only relevant near the edge of the first propagation threshold; the second term is exponentially decaying to zero as the size of the volume increases, and it comes solely from mode mixing and is contributed by the evanescent modes. Although this form of the correction term was derived for another system, it is nevertheless interesting to compare this formula for the conductor studied here.

In figure 6 we plot the correction term given by equation (18) together with $G_{111} + G_{112}$ which was computed using the right-hand side of equation (3), for the case where $H = W$. Equation (18) was evaluated using the scattering matrix elements obtained from our numerical calculation, and the system size $(x_2 - x_1)$ was specified as the length of our scattering volume $2L + 2W$ (see figure 1). For this conductor with $H = W$, we expect a good comparison with equation (18) which was derived for a δ-function scatterer inside a wire, because for both systems the geometric asymmetry is solely due to the position of the scattering volume boundary. Other than that, these systems are actually *symmetric* with respect to the scattering potential. Indeed, figure 6 clearly shows that there is essentially no

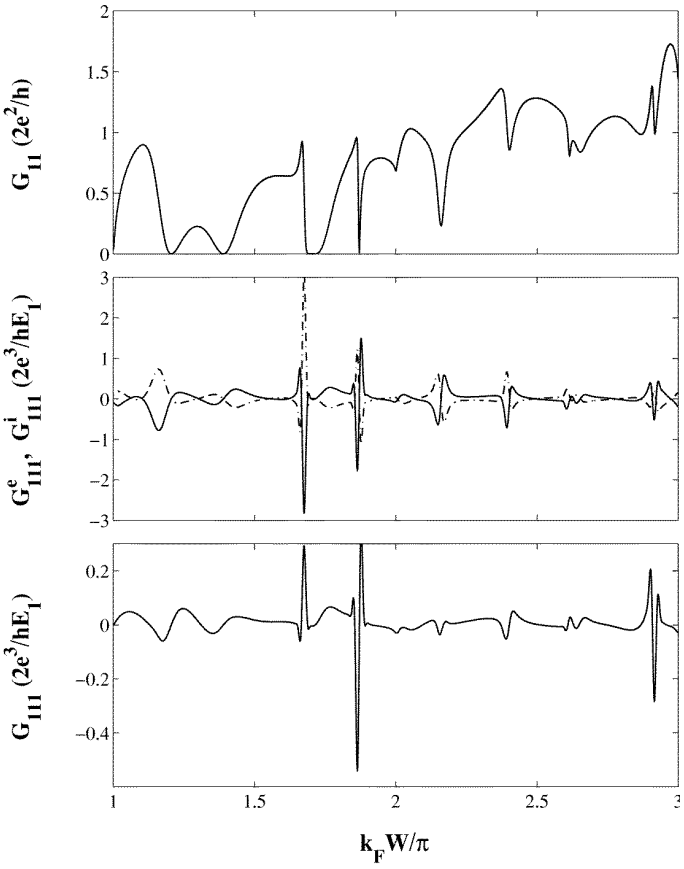

(d)

Figure 5. (Continued)

difference between equation (18) and our numerical data when the scattering volume is large ($L = 4W$). On the other hand, for a conductor with $H = 1.5W$ which has an intrinsically asymmetric scattering volume, the comparison is qualitative as shown in figure 7. However, the trends of the two curves are still similar. We may thus conclude that for the gauge-invariant condition, the correction term for the external contribution expression, equation (3), has a form of the same nature as that of equation (18) above.

5. Summary

In this work we have developed a numerical technique based on a scattering matrix to compute weakly non-linear conductance. This technique is particularly useful for conductors whose scattering volume can be naturally divided into several regions. The most difficult step is the evaluation of the local electric current response, namely the sensitivity. We have reported on how to obtain this quantity numerically; thus further investigations of the interesting non-linear conductance problem can be carried out using our numerical method. We have found that the sensitivity behaves differently when the transport energy is on and off resonance. The former leads to standing-wave-type spatial dependence, while the latter

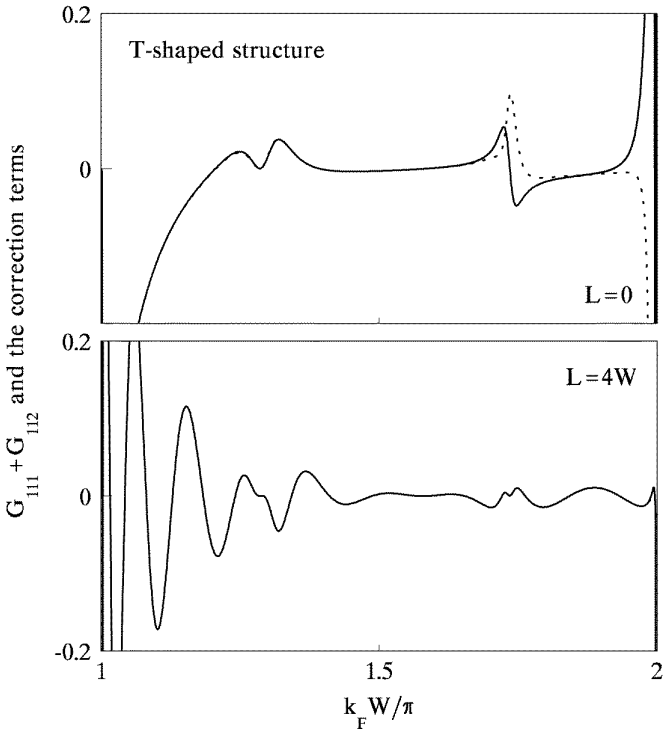

Figure 6. $G_{111}+G_{112}$ (solid line) and the correction term calculated according to equation (18) (dotted line) versus momentum for the T-shaped cavity ($H = W$). Upper panel: $L = 0$. Lower panel: $L = 4W$.

leads to a less regular behaviour. In all cases, the sensitivity shows a spatially oscillating pattern, which is similar to those known from exact calculations for 1D models.

The non-linear conductance can be non-zero only for geometrically asymmetric systems. The asymmetry can be introduced in two ways. The first is through the intrinsically asymmetrical shape of a conductor, such as that of figure 1 with $W < H < 2W$. The other, which is a trivial asymmetry, is introduced through the asymmetrical location of the scattering volume boundary, e.g. the case where $H = W$. We discovered that the intrinsic asymmetry leads to much larger non-linear conductance than the other case. Furthermore, for a symmetrical scattering junction but with asymmetrical location of the boundary (the $H = W$ case), for large size L the behaviour of the gauge-invariant condition agrees almost perfectly with equation (18) which was derived for a completely different system but also with the asymmetry introduced by means of the location of the scattering volume boundary only. On the other hand, such an agreement is less perfect for intrinsically asymmetrical systems. Hence we may conclude that the non-linear conductance behaves in quite different manners according to how the asymmetry is introduced.

The sign of the non-linear conductance can be positive or negative. Very sharp variations of this quantity are discovered at quantum resonances for the conductor studied here, where such resonances are marked by sharp reductions of the linear conductance G_{11}. Hence near a resonance, the electric current may actually decrease for an increasing voltage difference according to equation (1), since G_{111} is negative. Such a behaviour is precisely the expected non-linear conduction characteristic, and up to the second order in the voltage difference

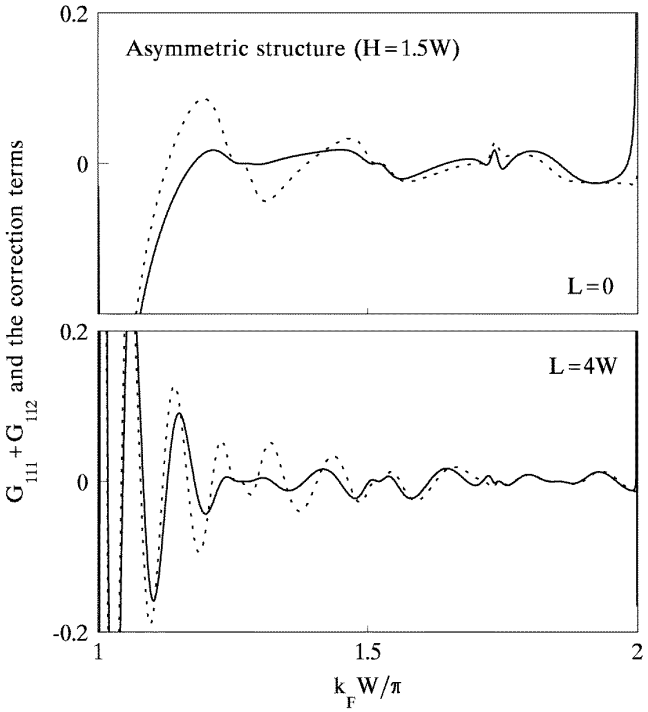

Figure 7. $G_{111}+G_{112}$ (solid line) and the correction term calculated according to equation (18) (dotted line) versus momentum for an asymmetric structure ($H = 1.5W$). Upper panel: $L = 0$. Lower panel: $L = 4W$.

our results can provide a prediction. Clearly, as the voltage difference becomes large, higher-order conductances must be included in order to obtain a meaningful prediction of the non-linear I–V curve. This is very important if one is to make quantitative comparisons with experimental data on the measured I–V characteristics of various 2D and 3D mesoscopic conductors. Because it is very difficult to perform gauge-invariant self-consistent calculations for non-linear transport for systems beyond 1D, our numerical method presented here gives a useful first step toward that goal.

Acknowledgments

We gratefully acknowledge support by a research grant from the Croucher Foundation, a RGC grant from the Hong Kong SAR under grant number HKU 7112/97P, a CRCG grant from the University of Hong Kong, the NSERC of Canada and FCAR of Québec. We thank the Computer Centre of the University of Hong Kong for computational facilities.

References

[1] Büttiker M 1993 *J. Phys.: Condens. Matter* **5** 9361
[2] Al'tshuler B L and Khmelnitskii D E 1985 *JETP Lett.* **42** 359
[3] Wingreen N S, Jauho A P and Meir Y 1993 *Phys. Rev.* B **48** 8487
[4] de Vegvar P G N 1993 *Phys. Rev. Lett.* **70** 837
[5] Taboryski R, Geim A K, Persson M and Lindelof P E 1994 *Phys. Rev.* B **49** 7813

[6] Büttiker M, Prêtre A and Thomas H 1993 *Phys. Rev. Lett.* **70** 4114
[7] Büttiker M, Thomas H and Prêtre A 1994 *Z. Phys.* B **94** 133
[8] Christen T and Büttiker M 1996 *Europhys. Lett.* **35** 523
[9] Wang J, Zheng Q R and Guo H 1997 *Phys. Rev.* B **55** 9763
[10] We thank Professor M Büttiker for pointing this out to us:
Büttiker M 1997 private communication
[11] The characteristic potential has been generalized to higher order. See
Ma Z S, Wang J and Guo H 1998 *Phys. Rev.* B **57** 9108
[12] Gasparian V, Christen T and Büttiker M 1996 *Phys. Rev.* A **54** 4022
[13] Büttiker M and Christen T 1996 *Quantum Transport in Semiconductor Submicron Structures* ed B Kramer (Dordrecht: Kluwer)
[14] Schult R L, Ravenhall D G and Wyld H W 1989 *Phys. Rev.* B **39** 5476
[15] Lee P A and Fisher D S 1981 *Phys. Rev. Lett.* **47** 882
[16] Baranger H U, DiVincenzo D P, Jalabert R A and Stone A D 1991 *Phys. Rev.* B **44** 10 637
[17] McLennan M J, Lee Y and Datta S 1991 *Phys. Rev.* B **43** 13 846
[18] Lent C S and Kirkner D J 1990 *J. Appl. Phys.* **67** 6353
[19] Wang Y J, Wang J and Guo H 1994 *Phys. Rev.* B **49** 1928
Leng M and Lent C S 1994 *J. Appl. Phys.* **76** 2240
[20] Sheng W D 1997 *J. Phys.: Condens. Matter* **9** 8369
[21] Tamura H and Ando T 1991 *Phys. Rev.* B **44** 1792
[22] Takagaki Y and Ferry D K 1992 *Phys. Rev.* B **45** 6716
[23] G^e_{111} was computed for figure 5 by replacing the energy derivatives of equation (3) with a potential derivative using the gauge-invariant condition. This procedure can be justified using the original formula given in references [13, 24] and numerically verified in reference [9].
[24] Leavens C R and Aers G C 1988 *Solid State Commun.* **67** 1135
Leavens C R and Aers G C 1989 *Phys. Rev.* B **39** 1202